Journal of Alloys and Compounds 505 (2010) 17–22

Contents lists available at ScienceDirect

Journal of Alloys and Compounds

journal homepage: www.elsevier.com/locate/jallcom

# On the existence of $ZrAs_2$ and ternary extension $Zr(Ge_xAs_{1-x})As$ ($0 \le x \le 0.4$)

Peter E.R. Blanchard, Ronald G. Cavell, Arthur Mar*

*Department of Chemistry, University of Alberta, Edmonton, Alberta, Canada T6G 2G2*

ARTICLE INFO

*Article history:*
Received 10 May 2010
Received in revised form 5 June 2010
Accepted 9 June 2010
Available online 18 June 2010

*Keywords:*
Arsenide
Solid solution
Crystal structure
Electronic structure
X-ray photoelectron spectroscopy

ABSTRACT

Zirconium diarsenide, $ZrAs_2$, has been established to be a genuine binary phase that is strictly stoichiometric. At 900 °C, it supports extensive solubility of Ge to form the ternary extension $Zr(Ge_xAs_{1-x})As$ ($0 \le x \le 0.4$). The crystal structures of $ZrAs_2$ and $Zr(Ge_{0.33(6)}As_{0.67})As$ were determined by single-crystal X-ray diffraction (orthorhombic $PbCl_2$-type, space group *Pnma*, $Z = 4$), with one of the two possible anion sites being preferentially occupied by the Ge atoms. X-ray photoelectron spectra and band structure calculations confirmed that the Ge and As atoms are anionic in character and that the substitution of Ge for As is driven by a depopulation of anion–anion antibonding states. $ZrGe_{0.3}As_{1.7}$ exhibits metallic behaviour and temperature-independent Pauli paramagnetism.



## 1. Introduction

Among the ternary M–Tt–Pn (M = Ti, Zr, Hf; Tt (tetrel) = Si, Ge, Sn; Pn (pnicogen) = P, As, Sb, Bi) systems, the antimonides are now relatively well studied whereas the other pnictides are not. One interesting outcome from these investigations has been the proposal that "β-$ZrSb_2$" does not exist as a true binary but rather as a Si-stabilized ternary phase, $Zr(Si_xSb_{1-x})Sb$, with a small phase width ($0.07 \le x \le 0.12$) adopting the orthorhombic $PbCl_2$-type structure [1]. With higher Si content, $ZrSi_{0.7}Sb_{1.3}$ forms the tetragonal PbFCl-type structure [2]. In both cases, the source of Si is believed to originate from the use of fused-silica tubes as the container material. Mixing of other Tt atoms (such as Ge and Sn) is also possible in these antimonides [1,2]. Similar doubts might be cast on the analogous binary $PbCl_2$-type zirconium arsenide, $ZrAs_2$, which was prepared in fused-silica tubes as well [3,4]. In an early structure determination, the possibility of an As-deficient formula, $ZrAs_{2-x}$, could not be excluded [4]. In more recent investigations, we have established that, like the antimonides, the ternary arsenides $Zr(Si_xAs_{1-x})As$ form a $PbCl_2$-type phase at lower Si content ($0 \le x \le 0.4$) (on the assumption that $ZrAs_2$ does exist) and a PbFCl-type phase at higher Si content ($x = 0.6$) [5].

Herein, we perform further experiments to determine if $ZrAs_2$ is indeed a true binary phase and to identify the phases formed in the As-rich portion of the ternary germanium-containing $Zr(Ge_xAs_{1-x})As$ system through X-ray diffraction analysis. As well, X-ray photoelectron spectroscopy (XPS), band structure calculations, and physical property measurements were carried out to characterize the electronic structures.

## 2. Experimental

### 2.1. Synthesis

Starting materials were Zr powder (99.9%), Ge pieces (99.99%), and As pieces (99.9998%), all from Alfa. Products were analyzed by powder X-ray diffraction (XRD) patterns obtained on an Inel diffractometer equipped with a CPS 120 detector.

Reactions with nominal loading composition "$ZrAs_2$" were carried out either directly in sealed fused-silica tubes or in alumina tubes jacketed by fused-silica tubes, with or without a small grain of $I_2$ (Anachemia) added to promote crystal growth, as summarized in Table 1. The tubes were evacuated, sealed, and placed in a furnace where they were heated to 850 °C over 2 days, kept at that temperature for 1 week, and cooled to room temperature over 1 day.

Similarly, reactions with loading compositions "$Zr(Ge_xAs_{1-x})As$" ($0 \le x \le 1$ at increments of 0.1–0.2) were carried out in alumina tubes jacketed by fused-silica tubes, which were evacuated and sealed. The tubes were heated at 500 °C for 1 day and 900 °C for 1 week, and then cooled to room temperature. The samples were ground and placed in new containers which were heated at 900 °C for 1 week. A few additional reactions were conducted at 1050 °C in attempts to prepare a PbFCl-type phase, to no avail.

### 2.2. Structure determination

Single-crystal X-ray diffraction data were collected on a Bruker Platform/SMART 1000 CCD diffractometer at 23 °C using $\omega$ scans. Structure solution and refinement were carried out with use of the SHELXTL (version 6.12) program package [6]. Face-indexed numerical absorption corrections were applied.

A needle-shaped single crystal was selected from the $ZrAs_2$ sample prepared in the silica-jacketed alumina tube in the presence of $I_2$. Although energy-dispersive X-ray (EDX) analysis performed on a Hitachi S-2700 scanning electron microscope indicated the presence of Zr and As, the absence of Si could not be directly ruled out because of the partial overlap of Zr L- and Si K-emission lines. From the intensity data, the orthorhombic space group *Pnma* was chosen and the initial atomic

* Corresponding author. Fax: +1 780 492 8231.
*E-mail address:* arthur.mar@ualberta.ca (A. Mar).

0925-8388/$ – see front matter © 2010 Elsevier B.V. All rights reserved.
doi:10.1016/j.jallcom.2010.06.049

**Table 1**
Reaction conditions and unit cell parameters for $ZrAs_2$.

| Reaction conditions | Products | $a$ (Å) | $b$ (Å) | $c$ (Å) | $V$ (Å$^3$) |
|---|---|---|---|---|---|
| Silica tube | $ZrAs_2$ | 6.800(2) | 3.687(1) | 9.036(3) | 226.3(2) |
| Silica tube, with $I_2$ | $ZrAs_2$ | 6.792(2) | 3.694(2) | 9.026(4) | 226.4(1) |
| Alumina tube | $ZrAs_2$ | 6.795(4) | 3.690(4) | 9.028(4) | 226.4(2) |
| Alumina tube, with $I_2$ | $ZrAs_2$ | 6.801(3) | 3.687(2) | 9.039(4) | 226.6(2) |

positions were located by direct methods. As an indirect test for the absence of Si, refinements were performed in which the two possible nonmetal sites were allowed to be occupied by a mixture of Si and As atoms, with no constraints over their ratio. The occupancies converged to 1(1)% Si and 99(1)% As on the first site (0.12, 1/4, 0.04), and 0(1)% Si and 100(1)% As on the second site (0.08, 1/4, 0.65), lending strong support for the absence of Si. In the final refinement, only As atoms were assumed to fully occupy these sites.

A needle-shaped single crystal was obtained from a reaction with nominal composition "$Zr(Ge_{0.4}As_{0.6})As$" prepared in the presence of $I_2$. Because the similar X-ray scattering factors of Ge and As posed a challenge in determining their site distribution, several models were tested. Placing Ge atoms entirely within the first site (0.12, 1/4, 0.04) and As atoms within the second site (0.08, 1/4, 0.65) resulted in equivalent isotropic displacement parameters, $U_{eq}$, of 0.0064(1) and 0.0073(1) Å$^2$, respectively, and agreement factors of $R(F) = 0.015$ and $R_w(F_o^2) = 0.034$. Reversing this site distribution gave $U_{eq}$ values of 0.0081(1) Å$^2$ for the first site and 0.0052(1) Å$^2$ for the second site, and slightly worse agreement factors of $R(F) = 0.016$ and $R_w(F_o^2) = 0.039$. Finally, a similar treatment as above in which Ge and As atoms were allowed to disorder over both sites was successful in resolving a preferential occupation of 37(8)% Ge and 63(8)% As on the first site, and 8(9)% Ge and 91(9)% As on the second site. Taking into account the large uncertainties in these occupancies, we assumed that only the first site was disordered with Ge and As atoms, whereas the second site was occupied exclusively by As atoms, in accordance with related structures such as $Zr(Ge_{0.2}Sb_{0.8})Sb$ and $Zr(Si_{0.4}As_{0.6})As$ in which the Tt atom enters only one of the two anion sites [1,5]. The final refinement led to a formula of "$Zr(Ge_{0.33(6)}As_{0.67})As$", which we simplify to $Zr(Ge_{0.3}As_{0.7})As$ in subsequent discussion.

Atomic positions were standardized with the program STRUCTURE TIDY [7]. Crystal data and further details of the data collection are given in Table 2. Final values of the positional and displacement parameters are given in Table 3. Selected interatomic distances are listed in Table 4. Further data, in CIF format, have been sent to Fachinformationszentrum Karlsruhe, Abt. PROKA, 76344 Eggenstein-Leopoldshafen, Germany, as supplementary material No. CSD-$_{421869}$ ($ZrAs_2$) and CSD-421870 ($Zr(Ge_{0.3}As_{0.7})As$) and can be obtained by contacting FIZ (quoting the article details and the corresponding CSD numbers).

### 2.3. Band structure calculations

Tight-binding linear muffin tin orbital (TB-LMTO) band structure calculations were performed on $ZrAs_2$ and hypothetical $Zr(Ge_{0.5}As_{0.5})As$ within the local density and atomic spheres approximations using the Stuttgart TB-LMTO program [8]. Cell parameters and atomic positions were taken from the crystal structures of $ZrAs_2$ and $Zr(Ge_{0.3}As_{0.7})As$. The ordered $Zr(Ge_{0.5}As_{0.5})As$ model (in space group $Pmc2_1$), based on one previously considered for $Zr(Si_{0.5}As_{0.5})As$ [5], involves an alternation of Ge and As atoms within zigzag chains parallel to $b$. The basis sets consisted of Zr 5s/5p/4d/4f, Ge 4s/4p/4d, and As 4s/4p/4d orbitals, with the Zr 4f, Ge 4d, and As 4d orbitals being downfolded. Integrations in reciprocal space were carried out with an improved tetrahedron method with 105 ($ZrAs_2$) or 168 ($Zr(Ge_{0.5}As_{0.5})As$) irreducible $k$ points within the first Brillouin zone.

### 2.4. X-ray photoelectron spectroscopy

XPS spectra were measured on a Kratos AXIS 165 spectrometer equipped with a monochromatic Al Kα X-ray source (15 kV, 14 mA) and a hybrid lens with a spot size of 700 μm × 400 μm. Crystals of $ZrAs_2$ or $Zr(Ge_{0.3}As_{0.7})As$ were ground into fine powder, pressed onto In foil, and mounted on a Cu sample holder. Although they did not appear to be air-sensitive, the samples were handled in a glove box and transferred within a sealed container to the XPS instrument. The pressure inside the analysis chamber was maintained at $10^{-7}$ to $10^{-9}$ Pa. The samples were sputter-cleaned with an $Ar^+$ ion beam (4 kV, 10 mA) until all surface oxides were removed. A slight reduction of As, caused by the sputtering procedure, does not detract from analysis of the As 3d spectra.

Survey spectra, which were collected with a binding energy (BE) range of 0–1100 eV, a pass energy of 160 eV, a step size of 0.7 eV, and a sweep time of 180 s, confirmed the expected compositions and, importantly, did not reveal the presence of Si in the samples. High-resolution core-line spectra were collected with an energy envelope of 60 eV (Zr 3d peak) or 20 eV (Ge 3d and As 3d peaks), a pass energy of 20 eV, a step size of 0.05 eV, and a sweep time of 180 s. No charge correction was applied because these samples are good conductors. All spectra were calibrated against the C 1s line at 284.8 eV arising from adventitious C. Although the C 1s signal overlaps with an As Auger signal, an acceptable method for checking the calibration in metallic systems such as these is to set the Fermi edge, located from the maximum of the first derivative of the valence band spectrum, to 0 eV [9]. The spectra were analyzed with use of the CasaXPS software package [10]. The background arising from energy loss was removed by applying a Shirley-type function

**Table 2**
Crystallographic data for $ZrAs_2$ and $Zr(Ge_{0.3}As_{0.7})As$.

| Formula | $ZrAs_2$ | $Zr(Ge_{0.33(6)}As_{0.67})As$ |
|---|---|---|
| Formula mass (amu) | 241.06 | 240.30 |
| Space group | *Pnma* (No. 62) | *Pnma* (No. 62) |
| $a$ (Å) | 6.8006(3) | 6.7380(4) |
| $b$ (Å) | 3.6883(2) | 3.6680(2) |
| $c$ (Å) | 9.0328(4) | 9.1202(5) |
| $V$ (Å$^3$) | 226.57(2) | 225.41(2) |
| $Z$ | 4 | 4 |
| $\rho_{calcd}$ (g cm$^{-3}$) | 7.067 | 7.081 |
| Crystal dimensions (mm) | 0.66 × 0.08 × 0.07 | 0.25 × 0.03 × 0.03 |
| $\mu$(Mo Kα) (mm$^{-1}$) | 33.38 | 33.07 |
| Transmission factors | 0.0235–0.1983 | 0.1123–0.5751 |
| $2\theta$ range (°) | 7.50–66.24 | 7.52–66.04 |
| No. of data collected | 2922 | 2882 |
| No. of unique data, including $F_o^2 < 0$ | 479 ($R_{int}$ = 0.037) | 476 ($R_{int}$ = 0.024) |
| No. of unique data, with $F_o^2 > 2\sigma(F_o^2)$ | 473 | 422 |
| No. of variables | 20 | 21 |
| $R(F)$ for $F_o^2 > 2\sigma(F_o^2)$[a] | 0.027 | 0.015 |
| $R_w(F_o^2)$[b] | 0.059 | 0.030 |
| Goodness of fit | 1.307 | 1.053 |
| $(\Delta\rho)_{max}$, $(\Delta\rho)_{min}$ (e Å$^{-3}$) | 2.29, −3.37 | 0.70, −0.94 |

[a] $R(F) = \sum ||F_o| - |F_c|| / \sum |F_o|$.

[b] $R_w(F_o^2) = \left[\sum [w(F_o^2 - F_c^2)^2] / \sum wF_o^4\right]^{1/2}$; $w^{-1} = [\sigma^2(F_o^2) + (Ap)^2 + Bp]$ where $p = [\max(F_o^2, 0) + 2F_c^2]/3$.

**Table 4**
Selected interatomic distances (Å) in $ZrAs_2$ and $Zr(Ge_{0.3}As_{0.7})As$[a].

| | $ZrAs_2$ | $Zr(Ge_{0.3}As_{0.7})As$ |
|---|---|---|
| Zr–*X*1 | 2.7727(4) | 2.7882(4) |
| Zr–As2 (×2) | 2.8030(3) | 2.8120(3) |
| Zr–*X*1 (×2) | 2.8133(3) | 2.8134(3) |
| Zr–As2 (×2) | 2.8374(3) | 2.8135(3) |
| Zr–*X*1 | 2.8759(5) | 2.8598(4) |
| Zr–As2 | 2.9560(4) | 2.9762(4) |
| *X*1–*X*1 (×2) | 2.5620(4) | 2.5635(4) |
| *X*1–As2 (×2) | 2.9017(4) | 2.8532(3) |

[a] Site *X*1 is occupied by As atoms in $ZrAs_2$ or by 0.3 Ge and 0.7 As in $Zr(Ge_{0.3}As_{0.7})As$.

**Table 3**
Atomic coordinates and equivalent isotropic displacement parameters for $ZrAs_2$ and $Zr(Ge_{0.3}As_{0.7})As$.

| Atom | Wyckoff position | Occupancy | $x$ | $y$ | $z$ | $U_{eq}$ (Å$^2$)[a] |
|---|---|---|---|---|---|---|
| $ZrAs_2$ | | | | | | |
| Zr | 4*c* | 1 | 0.22644(5) | 1/4 | 0.33804(3) | 0.0059(2) |
| As1 | 4*c* | 1 | 0.11820(5) | 1/4 | 0.04210(4) | 0.0072(2) |
| As2 | 4*c* | 1 | 0.08332(5) | 1/4 | 0.64704(3) | 0.0067(2) |
| $Zr(Ge_{0.3}As_{0.7})As$ | | | | | | |
| Zr | 4*c* | 1 | 0.22731(4) | 1/4 | 0.33785(3) | 0.0058(1) |
| Ge/As1 | 4*c* | 0.33(6)/0.67 | 0.11971(4) | 1/4 | 0.04266(3) | 0.0075(1) |
| As2 | 4*c* | 1 | 0.08873(4) | 1/4 | 0.64771(3) | 0.0070(1) |

[a] $U_{eq}$ is defined as one-third of the trace of the orthogonalized $U_{ij}$ tensor.

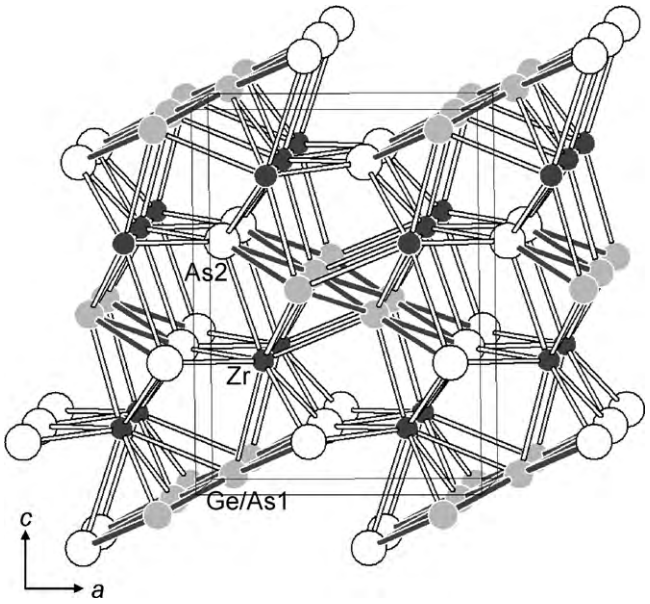


**Fig. 1.** $PbCl_2$-type structure of $ZrAs_2$ or $Zr(Ge_{0.3}As_{0.7})As$. The Ge atoms preferentially occupy only one of the two possible anion sites.

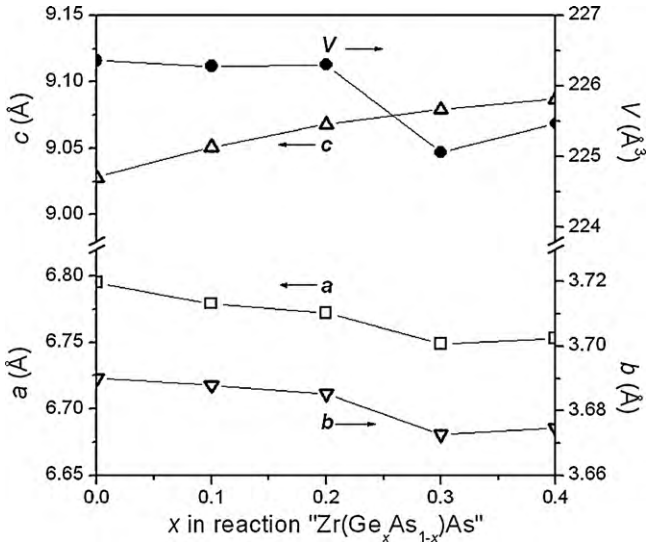


**Fig. 2.** Plot of cell parameters vs. $x$ for $Zr(Ge_xAs_{1-x})As$ forming the $PbCl_2$-type structure. The lines are shown only to guide the eye.

and the peaks were fitted to pseudo-Voigt (70% Gaussian and 30% Lorentzian) line profiles. On the basis of previous measurements made on the same spectrometer, the BE values are estimated to have a precision better than ±0.10 eV.

### 2.5. Electrical resistivity and magnetic susceptibility

A needle-shaped crystal of $Zr(Ge_{0.3}As_{0.7})As$ with dimensions of 0.60 mm × 0.015 mm × 0.015 mm was mounted for standard four-probe electrical resistivity measurements on a Quantum Design PPMS system equipped with an ac transport controller (Model 7100). The current was 100 μA and the frequency was 16 Hz. The resistivity was measured along the needle axis, which corresponds to the crystallographic $b$ axis, between 2 and 300 K.

Magnetic susceptibility measurements were made on a 100-mg ground sample of $Zr(Ge_{0.3}As_{0.7})As$ between 2 and 300 K on a Quantum Design 9T–PPMS dc magnetometer/ac susceptometer. The susceptibility was corrected for contributions from the holder and underlying sample diamagnetism.

## 3. Results and discussion

### 3.1. Is $ZrAs_2$ a true binary phase?

Reactions at 850 °C were carried out to prepare $ZrAs_2$ within different containers, in the presence or absence of $I_2$. Although EDX analyses on single crystals could not definitively rule out the absence of Si (because of the overlap of Zr and Si X-ray emission lines), the XPS survey spectra showed no evidence for Si. Powder X-ray diffraction revealed that the products of all these reactions were phase-pure (Fig. S1 in supplementary material). The refined cell parameters for the samples prepared within alumina tubes were within 3$\sigma$ from those prepared within silica tubes (Table 1). Single-crystal X-ray diffraction analysis indicated that the two anion sites are fully occupied by As atoms, with unremarkable displacement parameters. This body of evidence strongly supports the existence of $ZrAs_2$ as a strictly stoichiometric, true binary phase, and not an impurity-stabilized one, as has been proposed for "β-$ZrSb_2$" [1].

The structure of $ZrAs_2$ reported here ($R(F) = 0.027$) supersedes the earlier determination based on Weissenberg photographic data ($R(F) = 0.276$) [4]. The Zr atoms reside in approximately monocapped square antiprismatic polyhedra (CN9; Zr–As, 2.7727(4)–2.9560(4) Å), which are connected to form a three-dimensional network containing four-atom-wide anionic ribbons of As atoms extending along the $b$ direction (Fig. 1). Within these ribbons, the bonds within the interior (As1–As1, 2.5620(4) Å) are significantly shorter than those to the terminal atoms (As1–As2, 2.9017(4) Å).

### 3.2. Ternary extension $Zr(Ge_xAs_{1-x})As$.

Reactions performed at 900 °C indicated that the solid solution $Zr(Ge_xAs_{1-x})As$ forms for $0 \le x \le 0.4$. Powder X-ray diffraction patterns revealed phase-pure products up to $x = \sim 0.4$ (Table S1 and Fig. S2 in supplementary material). A crystal obtained from a reaction with nominal composition "$Zr(Ge_{0.4}As_{0.6})As$" was found from the single-crystal structure determination to have a formula of $Zr(Ge_{0.33(6)}As_{0.67})As$, with the Ge atoms preferentially entering the interior sites of the four-atom-wide anionic ribbons. The uncertainties in the occupancies are large enough that the upper limit of Ge solubility into $ZrAs_2$ can be estimated to be no higher than $x = 0.4$. Above this point, multiphase mixtures consisting of $PbCl_2$-type $Zr(Ge_xAs_{1-x})As$, ZrAs, and elemental Ge were observed. A Ge-rich phase of approximate composition "$ZrGe_{1.3}As_{0.7}$" was identified which probably lies off the $ZrAs_2$–$ZrGe_2$ join in the ternary phase diagram; further investigation of this phase was hampered by lack of suitable crystals for structure determination.

On most scales of atomic radii, Ge is slightly larger than As (e.g., Pauling metallic radii $R_1$ of 1.24 Å for Ge and 1.21 Å for As) [11]. At first glance, it is somewhat surprising, then, to observe that the unit cell volume contracts slightly (by 1 $Å^3$) on progressing from $ZrAs_2$ to $Zr(Ge_{0.4}As_{0.6})As$ (Fig. 2). The small change in unit cell volume results from the trends of decreasing $a$ and $b$ opposing the trend of increasing $c$. These trends cannot be easily explained by geometrical considerations. An argument based on size effects would also need to take into account that the Ge and As atoms are anionic but with differing charges. The Zr–$X1$ (where $X1$ is the disordered site) and Zr–As2 distances change irregularly as Ge partially substitutes for As (Table 4), such that the average bond lengths around the Zr atom remain unchanged at 2.83 Å. Within the four-atom-wide anionic ribbons (As2–$X1$–$X1$–As2), the $X1$–$X1$ distances remain the same whereas the $X1$–As2 distances shorten. In TiNiSi-type structures, which are ternary variants of the $Co_2Si$-type (anti-$PbCl_2$-type) structure, the interior sites of these ribbons tend to be occupied by smaller atoms [12]. If the same argument is applied to $Zr(Ge_{0.4}As_{0.6})As$, then the preference for Ge atoms to enter the interior $X1$ sites implies that the Ge atoms are smaller and

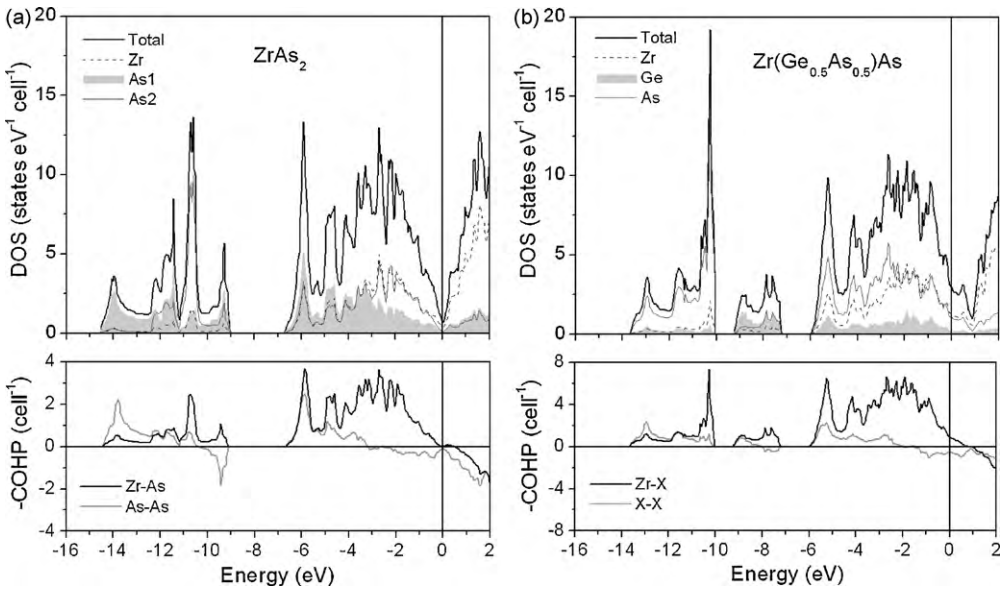


**Fig. 3.** Band structures for (a) $ZrAs_2$ and (b) hypothetically ordered "$Zr(Ge_{0.5}As_{0.5})As$". The top panels show the density of states (DOS) and atomic projections. The bottom panels show the crystal orbital Hamilton population (–COHP) curves.

less negatively charged than the As atoms, thereby accounting for the cell contraction.

### 3.3. Electronic structure and physical properties

Because the trends in bond lengths suggest that electronic effects are at play, the band structures for $ZrAs_2$ and a hypothetically ordered model of $Zr(Ge_{0.5}As_{0.5})As$ were examined. The lowest energy block (from −14.5 to −9 eV) in $ZrAs_2$ splits into two subbands upon the ordered substitution of Ge into one of the As sites in $Zr(Ge_{0.5}As_{0.5})As$ (Fig. 3). At higher energy, the density of states (DOS) curves are similar except that the Fermi level is shifted from its position at a pseudogap in $ZrAs_2$ to just slightly below (by 1 eV) in $Zr(Ge_{0.5}As_{0.5})As$, a consequence of the reduced electron count. Inspection of the crystal orbital Hamilton population (COHP) curves in $ZrAs_2$ reveals that Zr–As bonding is optimized but As–As bonding is not because some antibonding levels are occupied (Fig. 3). Lowering the Fermi level in $Zr(Ge_{0.5}As_{0.5})As$ depopulates these anion–anion antibonding states. As judged from the integrated COHP values (–ICOHP), this has little effect on the *X*1–*X*1 bonds (1.8 eV in both $ZrAs_2$ and $Zr(Ge_{0.5}As_{0.5})As$) but strengthens the *X*1–As2 bonds (0.4 eV in $ZrAs_2$ vs. 0.6 eV in $Zr(Ge_{0.5}As_{0.5})As$). This stabilization of anion–anion bonding competes with the destabilization of Zr–anion bonding, setting a limit on how much Ge can substitute for As. In $Zr(Ge_{0.5}As_{0.5})As$, the Zr–anion bonding interactions near the Fermi level are quite weak such that the –ICOHP value remains essentially unchanged (1.5 eV) from that in $ZrAs_2$.

The electronic character of these compounds was further examined through XPS analysis. Because the Ge 3d and Zr 4p

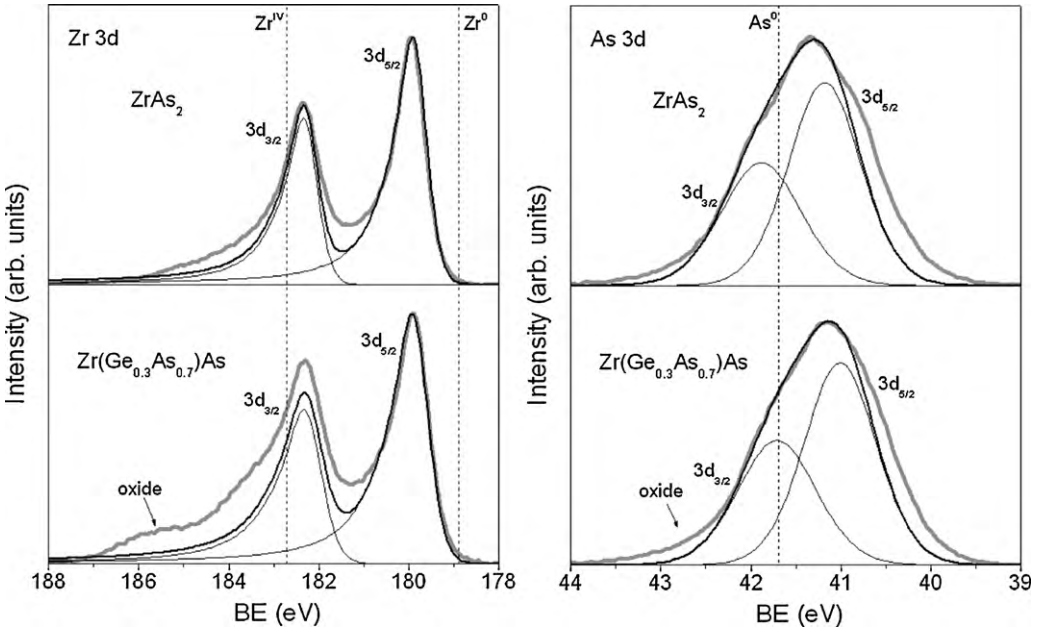


**Fig. 4.** (a) Zr 3d and (b) As 3d XPS spectra for $ZrAs_2$ (top panels) and $Zr(Ge_{0.3}As_{0.7})As$ (bottom panels). The experimental spectra (thick grey lines) are fitted with component peaks (thin lines) to give the combined envelope (black lines). The dashed vertical lines mark the Zr $3d_{5/2}$ and As $3d_{5/2}$ BEs expected for the indicated charges.

peaks overlap, we present only the Zr 3d and As 3d XPS spectra for $ZrAs_2$ and $Zr(Ge_{0.3}As_{0.7})As$. In both compounds, the Zr 3d spectra were fitted to two peaks corresponding to the $3d_{5/2}$ and $3d_{3/2}$ spin–orbit-coupled final states, with an intensity ratio of 3:2 (Fig. 4a). The shoulder at high BE, quite prominent in $Zr(Ge_{0.3}As_{0.7})As$, is attributed to surface oxides. The asymmetric lineshapes are a signature of electronic delocalization, as described previously [13]. The Zr $3d_{5/2}$ BE of 179.9(1) eV, identical for $ZrAs_2$ and $Zr(Ge_{0.3}As_{0.7})As$, falls between those for Zr metal (178.9(3) eV) and $ZrO_2$ (182.7(6) eV) [14], indicating the presence of cationic Zr species with an intermediate oxidation state consistent with partially filled Zr 3d states found in the DOS curves. The As 3d spectra suffer from a slight reduction, common in the spectra for other arsenides [15,16], caused by $Ar^+$ sputtering giving rise to the shoulders at low BE; surface oxides probably give rise to the shoulders at high BE (Fig. 4b) [17]. These spectra were fitted to two component peaks corresponding to the $3d_{5/2}$ and $3d_{3/2}$ spin–orbit-coupled final states separated by 0.7 eV, each with a FWHM of 1.0 eV and in an intensity ratio of 3:2. The As $3d_{5/2}$ BE (41.2(1) eV for $ZrAs_2$ and 41.0(1) eV for $Zr(Ge_{0.3}As_{0.7})As$) is lower than in elemental As (41.7(2) eV), indicating the presence of anionic As species with a charge close to 1−, as deduced by comparison to the spectra of related compounds [14]. The BE is slightly lower in $Zr(Ge_{0.3}As_{0.7})As$ than in $ZrAs_2$, which would be consistent with the expectation of more negatively charged As atoms induced by the greater polarity of Ge–As bonds, but we cannot rule out the possibility that the small shift may be spurious, perhaps caused by the $Ar^+$ sputtering.

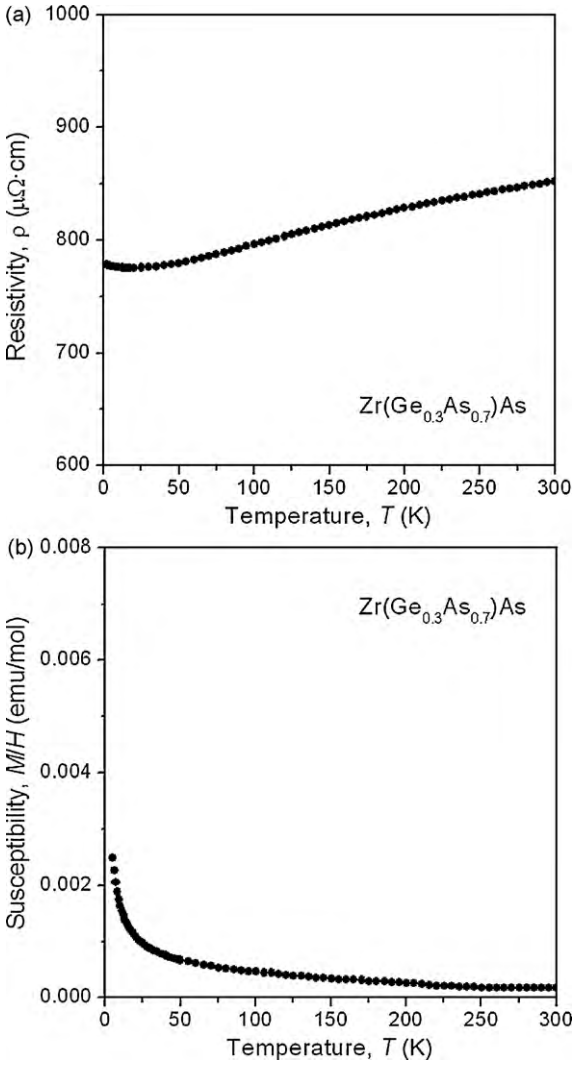


**Fig. 5.** (a) Electrical resistivity and (b) magnetic susceptibility for $Zr(Ge_{0.3}As_{0.7})As$.

Consistent with the band structure, $Zr(Ge_{0.3}As_{0.7})As$ exhibits weakly metallic behaviour. The high electrical resistivity and the low residual resistivity ratio ($\rho_2/\rho_{300} = 0.9$) stem from the disorder in this compound (Fig. 5a). The magnetic susceptibility curve indicates temperature-independent Pauli paramagnetism, with a small Curie tail presumably due to trace impurities (Fig. 5b).

## 4. Conclusions

Unlike the antimonide "β-$ZrSb_2$", which is impurity-stabilized, the arsenide $ZrAs_2$ is a true binary phase adopting the $PbCl_2$-type structure. The ternary extension $Zr(Ge_xAs_{1-x})As$ forms up to $x = \sim 0.4$, with Ge atoms entering preferentially into the interior sites of four-atom-wide anionic ribbons in this structure. This solid solution range is similar as observed previously in $Zr(Si_xAs_{1-x})As$ but is much wider than in $Zr(Si_xSb_{1-x})Sb$ [1,5]. Although the substitution of Si or Ge into $ZrAs_2$ seems to originate for the same reasons (strengthened anion–anion bonding) as for the impurity stabilization of "β-$ZrSb_2$", there are subtle differences in these systems that may need to be explored further. Curiously, for example, a PbFCl-type phase was not observed in $Zr(Ge_xAs_{1-x})As$ with higher values of $x$, unlike $Zr(Si_xAs_{1-x})As$ or $Zr(Si_xSb_{1-x})Sb$, at least under the temperatures studied (from 900 to 1050 °C). The band structure of $ZrAs_2$ reveals a pseudogap at the Fermi level and the electrical resistivity of $Zr(Ge_{0.3}As_{0.7})As$ is quite high, characteristic of a poor metal. These features suggest that the thermal properties of $ZrAs_2$ or related pnictides may be worthwhile investigating towards potential applications in thermoelectric materials.

## Acknowledgments

The Natural Sciences and Engineering Research Council (NSERC) of Canada supported this work. P.E.R.B. thanks NSERC and Alberta Ingenuity for scholarship support. Dr. Robert McDonald and Dr. Michael J. Ferguson (X-ray Crystallography Laboratory) performed the X-ray data collection, and Ms. Christina Barker (Department of Chemical and Materials Engineering) assisted with the EDX analysis. Access to the Kratos AXIS 165 XPS spectrometer was provided by the Alberta Centre for Surface Engineering and Science (ACSES), which was established with support from the Canada Foundation for Innovation and from Alberta Innovation and Science.

## Appendix A. Supplementary data

Supplementary data associated with this article can be found, in the online version, at doi:10.1016/j.jallcom.2010.06.049.

## References

[1] N. Soheilnia, A. Assoud, H. Kleinke, Inorg. Chem. 42 (2003) 7319–7325.
[2] R. Lam, A. Mar, J. Solid State Chem. 134 (1997) 388–394.
[3] W. Trzebiatowski, S. Węglowski, K. Łukaszewicz, Rocz. Chem. 30 (1956) 353–354.
[4] W. Trzebiatowski, S. Węglowski, K. Łukaszewicz, Rocz. Chem. 32 (1958) 189–201.
[5] M.W. Gaultois, A.P. Grosvenor, P.E.R. Blanchard, A. Mar, J. Alloys Compd. 492 (2010) 19–25.
[6] G.M. Sheldrick, SHELXTL, Version 6.12, Bruker AXS Inc., Madison, WI, 2001.
[7] L.M. Gelato, E. Parthé, J. Appl. Crystallogr. 20 (1987) 139–143.
[8] R. Tank, O. Jepsen, A. Burkhardt, O.K. Andersen, TB-LMTO-ASA Program, Version 4. 7, Max Planck Institut für Festkörperforschung, Stuttgart, Germany, 1998.
[9] D. Briggs, Surface Analysis of Polymers by XPS and Static SIMS, Cambridge University Press, Cambridge, UK, 2005.
[10] N. Fairley, CasaXPS, Version 2.3.9, Casa Software Ltd., Teighnmouth, Devon, UK, 2003, http://www.casaxps.com.
[11] L. Pauling, The Nature of the Chemical Bond, 3rd ed., Cornell University Press, Ithaca, NY, 1960.

[12] G.A. Landrum, R. Hoffmann, J. Evers, H. Boysen, Inorg. Chem. 37 (1998) 5754–5763.
[13] S. Doniach, M. Šunjić, J. Phys. C: Solid State Phys. 3 (1970) 285–291.
[14] C.D. Wagner, A.V. Naumkin, A. Kraut-Vass, J.W. Allison, C.J. Powell, J.R. Rumble Jr., NIST X-ray Photoelectron Spectroscopy Database, Version 3.5 (Web Version), National Institute of Standards and Technology, Gaithersburg, MD, 2003, http://srdata.nist.gov/xps.
[15] A.P. Grosvenor, R.G. Cavell, A. Mar, J. Solid State Chem. 181 (2008) 2549–2558.
[16] P.E.R. Blanchard, B.R. Slater, R.G. Cavell, A. Mar, A.P. Grosvenor, Solid State Sci. 12 (2010) 50–58.
[17] A. Siokou, M. Kalyva, S.N. Yannopoulos, M. Frumar, P. Němec, J. Phys.: Condens. Matter 18 (2006) 5525–5534.